order to take Full advantage of this could be taken in the trigger, if the readout is done faster (a higher bus speed is likely achievable). For example, more parallel processors could be introduced at the module level such as two DSPs per module.

Although this is a new solution to the readout of PC, not much development is needed to determine the performance of such a system. Tests with this pad geometry need to be performed on a small test chamber. Important questions to be answered are: What is the efficiency to have three adjacent pads fired? What is the probability that noise produces three fired pads? Can a position resolution better than the pad width be achieved?

Most questions on backplane construction, such as COB mounting and chip design, will be answered during the winter of 1992–93, when the prototyping of a pad readout module for a multistep avalanche chamber will be made by the University of Lund group together with the chip design company (SiCon, Linköping, Sweden) and the COB company (XICON, Malmö, Sweden). An operating prototype is expected by May 1993.

6.4 Time Expansion Chamber

The time expansion chamber (TEC) performs both particle identification and tracking functions in PHENIX. Through measurement of charged particle ionization energy losses (dE/dx) the detector allows separation of electrons from pions over a momentum range of 250 MeV/c to 3.0 GeV/c. The detector also tracks all charged particles in the region between the RICH and the EMCal, producing direction vectors that are matched with track information in the drift chambers and pad chambers to complete track determination. The basic design of the TEC is shown in Fig. 6.21.

6.4.1 Mechanical Design

The detector consists of four planes of wire chambers built in two flat 45° segments in each arm. The TEC occupies the region where the inscribed radius from the vertex is between 4.10 m and 4.57 m and has an active area that covers $\eta = \pm 0.35$. Each wire chamber contains an aluminized mylar window followed by a 3-cm drift space, a plane of cathode wires, a plane of anode wires and a final aluminized mylar window (Fig. 6.22). The anode wires are spaced 4 mm from each other and 3 mm from the both the cathode wire plane and the aluminized mylar window. The wires are oriented parallel to the z-axis direction of the detector and have lengths increasing from 3.00 m to 3.24 m as the detector planes increase in radius. Each anode wire is divided in half at its midpoint to decrease the occupancy per wire. The active area of the largest 45° segment is 3.67×3.24 m^2. The frames of the detector are made from a combination of G-10 and carbon-fiber members. The anode wires are divided in z by running a thin cross piece of G-10 underneath all the wires at their midpoints, epoxying the wires to the cross piece with two parallel beads of epoxy separated by a few millimeters and cutting the wires in between the two beads.

The anode and cathode wires run to the edge of the detector frame where they are glued to the frame with epoxy and soldered to printed circuit boards laminated to the frames. Traces on the PC board route the anode signals to multichip modules (MCM) mounted

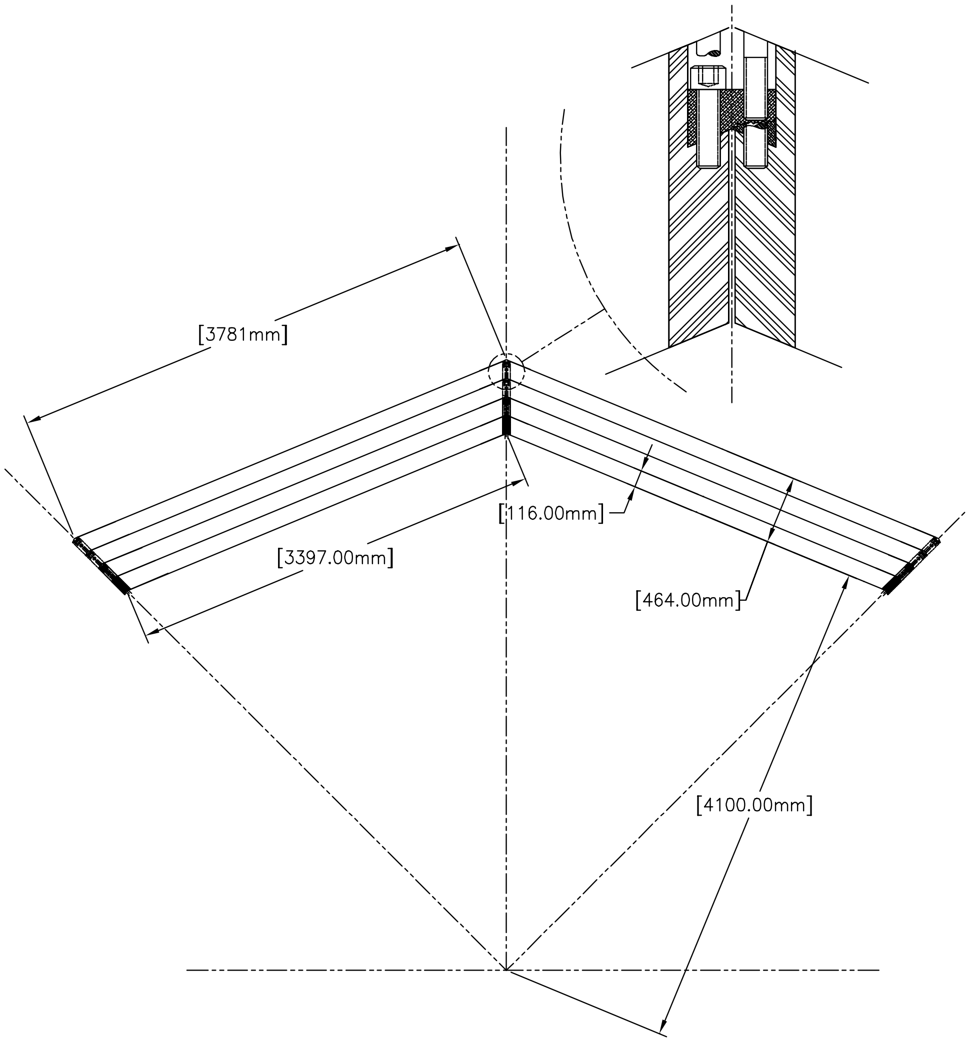

Figure 6.21: Diagram of TEC showing overall dimensions and frame locations.

on the motherboard. The electronics in the MCM will include the preamplifier, shaping amplifier, Flash ADC and memory buffer.

The TEC will initially run with an argon based gas mixture that will allow good tracking performance and $dE/$dx particle separation. It will be operated with a drift velocity (v_d) in the range of 15–50 mm/μs and a gas gain on the order of 10^4. When the detector is upgraded to a TRD/TEC (see Chapter 15), a xenon-ethane-based mixture will be used to both enhance the dE/dx performance and allow the efficient detection of transition radiation x-rays.

Each plane of the TEC is separated from the next by a distance of 8 cm. This space will be filled by the radiator of the TRD. Space has also been left between the fourth plane of the TEC and the TOF wall for the addition of two more TEC planes. When the upgrade is complete the TEC subsystem will be a six-plane TRD-dE/dx detector with e/π separation of

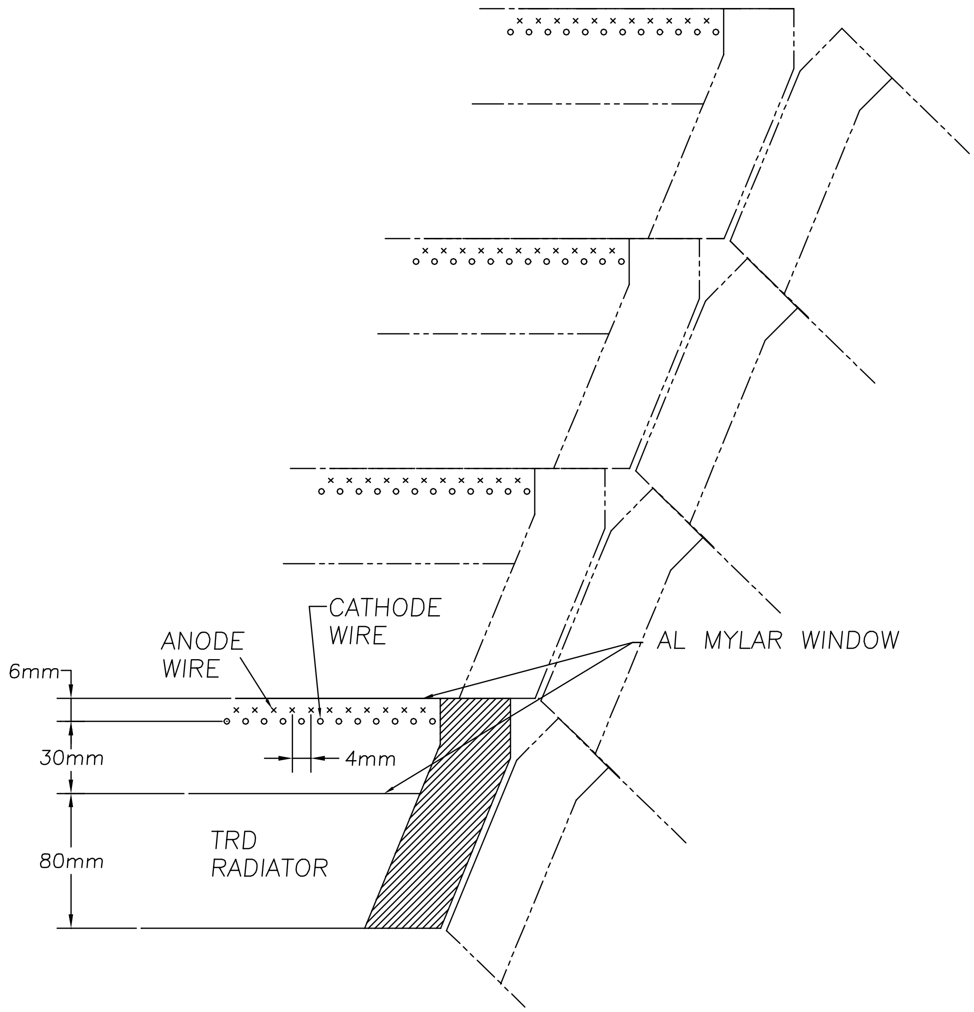

Figure 6.22: TEC schematic showing wire position, drift volume and radiator location.

better than 2×10^{-3} over a momentum range starting at 250 MeV/c and continuing beyond 50 GeV/c.

6.4.2 Electronics

The TEC electronics chain consists of a preamplifier followed by a 70 ns shaping amplifier, a 4-bit nonlinear FADC running at 40 MHz, and an IC containing a buffer plus data compression processing (Fig. 6.23). The parameters of the electronics chain are determined by requirements of both the TEC dE/dx and the TRD operation. The 70 ns shaping is chosen so that the FADC clock runs at a fraction of the shaping time to assure good position resolution. The shaping time is also appropriate for transition radiation measurements, where the shaping time chosen will allow the containment of the total signal from the TR x-ray absorbed in the gas chamber. The output of the shaper is split with part of the signal going

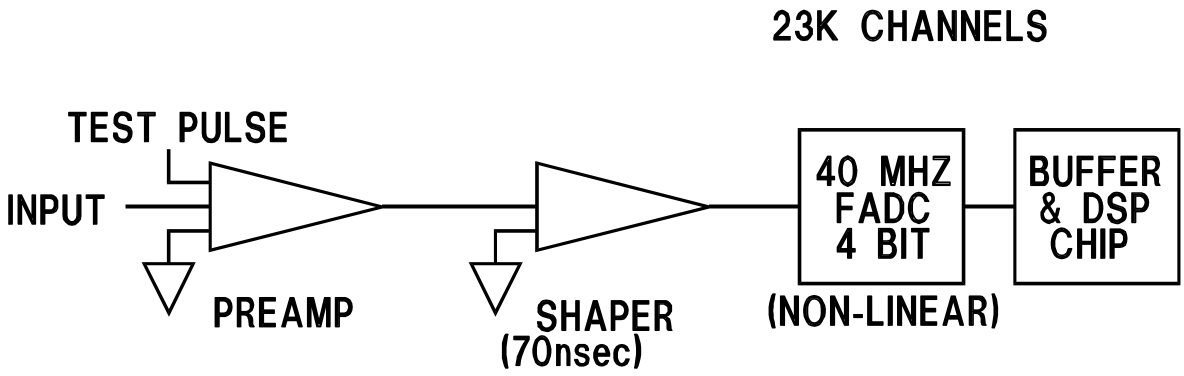

Figure 6.23: TEC electronics chain of preamplifier, shaping amplifier, FADC and buffer.

directly into a 2-bit FADC, and the rest of the signal going through another $\times 10$ amplifier stage and then into the 4-bit FADC. The signal is split so that the FADC has sensitivity both for low dE/dx signal (0.2–0.3 keV for Xe gas), and the transition radiation signal (3–10 keV for Xe). Without this signal splitting scheme an 8-bit FADC would be needed to cover the dynamic range required by the detector. The exact cycle time of the FADC clock will be chosen to be an integral fraction of the crossing time. The many ADC samples given by the FADC enhance the particle identification from both dE/dx and TR by providing information on track energy deposit versus chamber position. Results from a test run with a tracking TRD prototype (Fig. 6.24) show that a 4-bit FADC is adequate for good particle identification. In the figure 6.24 the S value is defined as:

$$S = \frac{(E_e - E_\pi) - 2\sigma_e(E_\pi/E_e)}{\sigma_\pi}$$

E_e and E_π represent the means of the dE/dx truncated mean distribution for electrons and pions.

A CMOS IC prototype containing the preamplifier and shaping amplifier has already been produced by the BNL Instrumentation group (Fig. 6.25). Design work is underway on the FADC chip with individual components of the chip already having been submitted to an IC foundry for prototype fabrication.

The ASIC containing the preamplifier and shaping amplifier will contain four to eight channels/chip and be manufactured with the 2 μm n-well CMOS process. The shaping function is unipolar, with a semi-Gaussian impulse response, 70 ns peaking time and a FWHM $<$ 100 ns. The ENC is less than 1500 electrons for 70 ns shaping and a 30–40 pf input capacitance (Fig. 6.26). The chip requires ± 2.5 V. Its output is 2 V full scale.

Most of the ENC noise comes from the preamp input device so special attention has been paid to its design and biasing. The ASIC ENC has been kept low by using a minimum gate length, paying careful attention to the gate and substrate parasitic resistances, and reverse biasing the source-substrate junction.

A 4-bit, 40 MHz, FADC has been designed, simulated, and layed-out in 2 μm double-

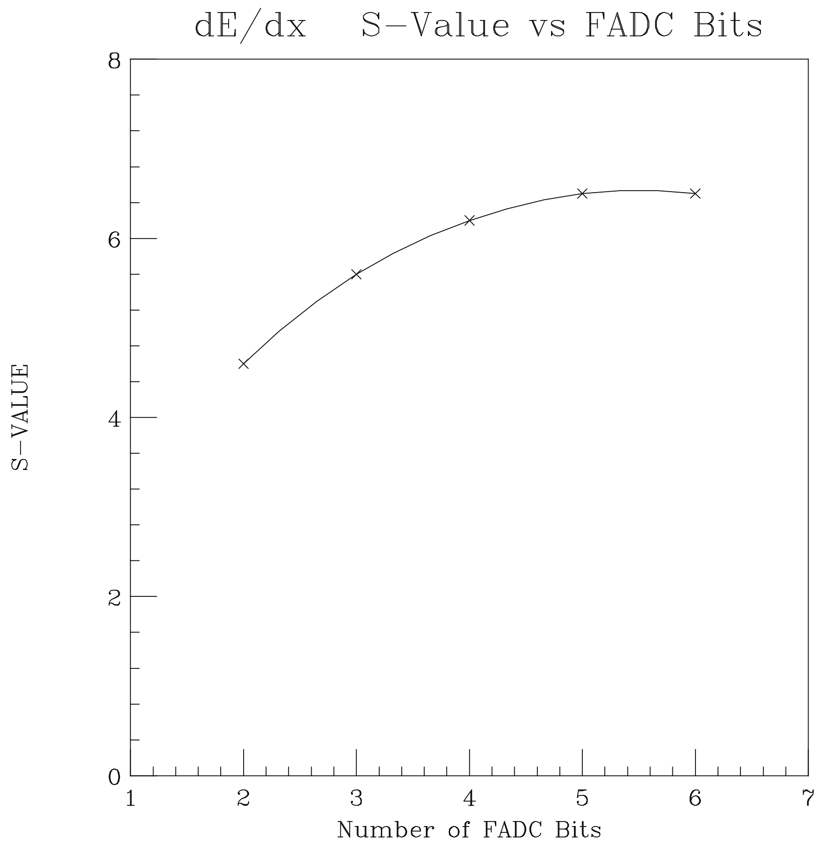

Figure 6.24: S-value for e/π rejection vs. number of ADC bits.

poly CMOS technology. The circuit operates from a single 5 V power supply and should dissipate less than 100 mW of power at full speed. The input signal voltage range is equal to the power supply rails (0–5 V) and the absolute accuracy of the ADC should be better than 20 mV *rms*. The overall size of the circuit is approximately 1 mm^2 allowing many such circuits to be placed on a single die. The circuit may be optimized for speed, accuracy, or power with only modest modifications to the layout.

The operation of the FADC is illustrated in the simplified block diagram of Fig. 6.27. The input signal is applied to all 16 comparators, along with individual reference voltages from the resistive ladder network. Each comparator decides whether or not the input signal exceeds its respective reference voltage. A digital logic level of one is produced if this condition is true. A logic level of zero is produced otherwise. This information is stored in a register and applied to an encoder that produces a 4-bit binary-coded output. This information is again stored in a register and driven off-chip, completing the conversion cycle. The multiphase clock generator provides the necessary timing signals to synchronize the operations just described.

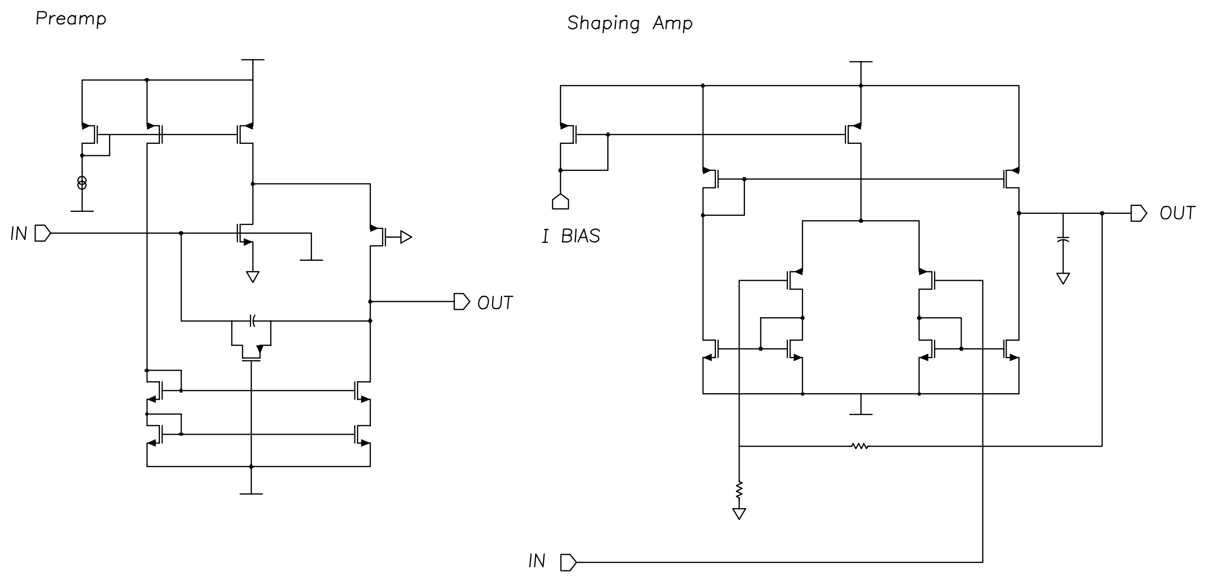

Figure 6.25: Circuit diagram of TEC preamplifier and shaping amplifier prototypes. They have been manufactured using 2 μm n-well CMOS process.

For reasons of clarity, each comparator is shown as a simple block. In reality, each comparator contains *auto-zeroing* circuitry that improves accuracy by reducing internal offset errors. In addition, each comparator has its own track-and-hold circuitry that improves input analog bandwidth. This bandwidth should exceed 20 MHz.

6.4.3 Operation and Performance

The four plane TEC is designed to have single point track resolution of 200–250 μm in the r-ϕ direction and two track separation of about 2 mm for tracks normal to the detector. The dE/dx measurement capability will allow e/π separation of 5×10^{-3} at 600 MeV/c and 2×10^{-2} at 2.0 GeV/c. Each detector plane has a total radiation length of 0.06%.

The operation of the TEC in PHENIX can best be understood by considering a TPC whose drift is radial rather than axial. When a charged track traverses a TEC plane the track ionizes the gas along its path and the electron clusters from the ionization begin to drift radially toward the anode wires (Fig. 6.28). The electric field geometry in the TEC is such that the field lines are parallel in the drift region with the lines of constant drift time being almost straight across a wire cell. This field configuration results in the arrival time of electron clusters at the anode being proportional to the radial position (r) in the drift region

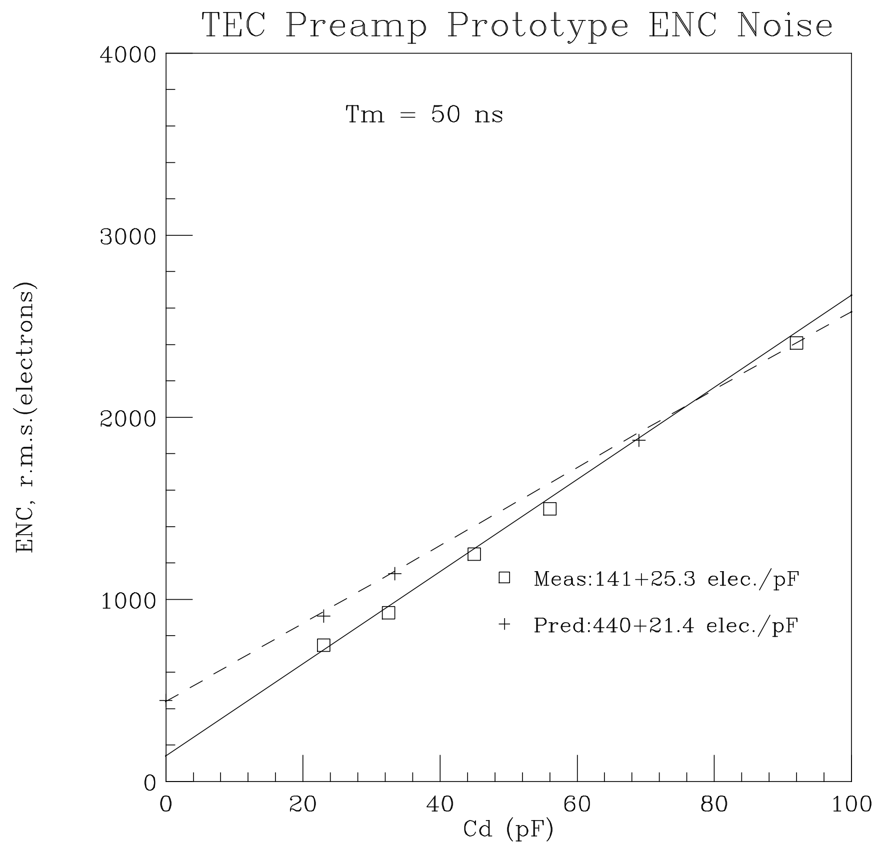

Figure 6.26: ENC vs. input capacitance for TEC preamp.

at which they were created. The arrival time at the anode wires is measured with 40 MHz FADC electronics. For tracks in each cell the leading and trailing edge time is recorded. The leading edge time is proportional to the r position at which the track crossed the cell boundary. From this information, the position of the crossing point in r and r-ϕ can be determined with an accuracy of 200–250 μm. The resolution in the drift region is primarily limited by the diffusion of the electron cluster in the gas. Every time a track crosses a wire cell boundary an independent position in r and r-ϕ is measured for the track. Also, the number of time slices for each track is inversely proportional to the track-angle through the drift cell. The r-ϕ position and track-angle information is combined to yield track direction-vector information in each TEC plane. Tracks that traverse the proportional region of a wire cell have their leading-edge time depend on the distance of closest approach the anode wire. The field shape in the proportional region is approximately cylindrical. Tracks in this region have their r-ϕ position measure to an accuracy of 200–250 μm. The resolution in this region is limited by the time resolution of the FADC. The track resolutions have been measured with a prototype TEC.

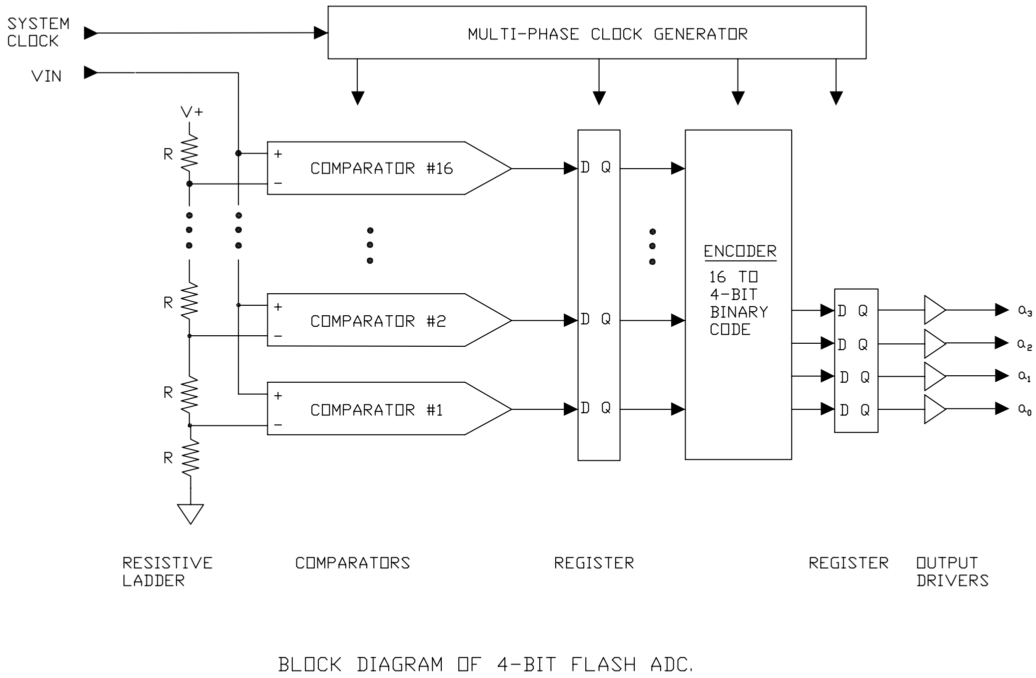

Figure 6.27: Block diagram of TEC FADC showing 16 comparators and a 4-bit encoder. A 2 μm CMOS prototype is being produced.

The energy loss information located in each time bucket of the FADC can be used to effectively distinguish electrons from pions at momenta between 0.25 GeV/c and about 3.0 GeV/c. In this momentum range the relativistic rise of the electron dE/dx curve causes the electron to lose more energy through dE/dx than a pion loses. By making a distribution of the ADC information in each FADC bucket for each track, and then taking a truncated mean, the electrons from less relativistic particles are distinguished in the TEC. Both simulations and measurement with PHENIX prototype detectors have been used to establish the expected e/π separation.

Having good track resolution and two track separation are important in the TEC because the ability to identify all tracks is necessary to minimize degradation of particle identification performance due to overlapping tracks. In environments of high track density, the particle identification aspects of the detector may degrade when overlap of dE/dx energy loss from two or more tracks combine to look like the energy deposit of a particle which is on the relativistic rise part of the dE/dx curve. High quality tracking, where all tracks are identified, helps to eliminate this problem.

Both detailed simulations and measurements with prototype detectors have been performed for the PHENIX TEC. The prototype tests took place in a secondary beam of pions

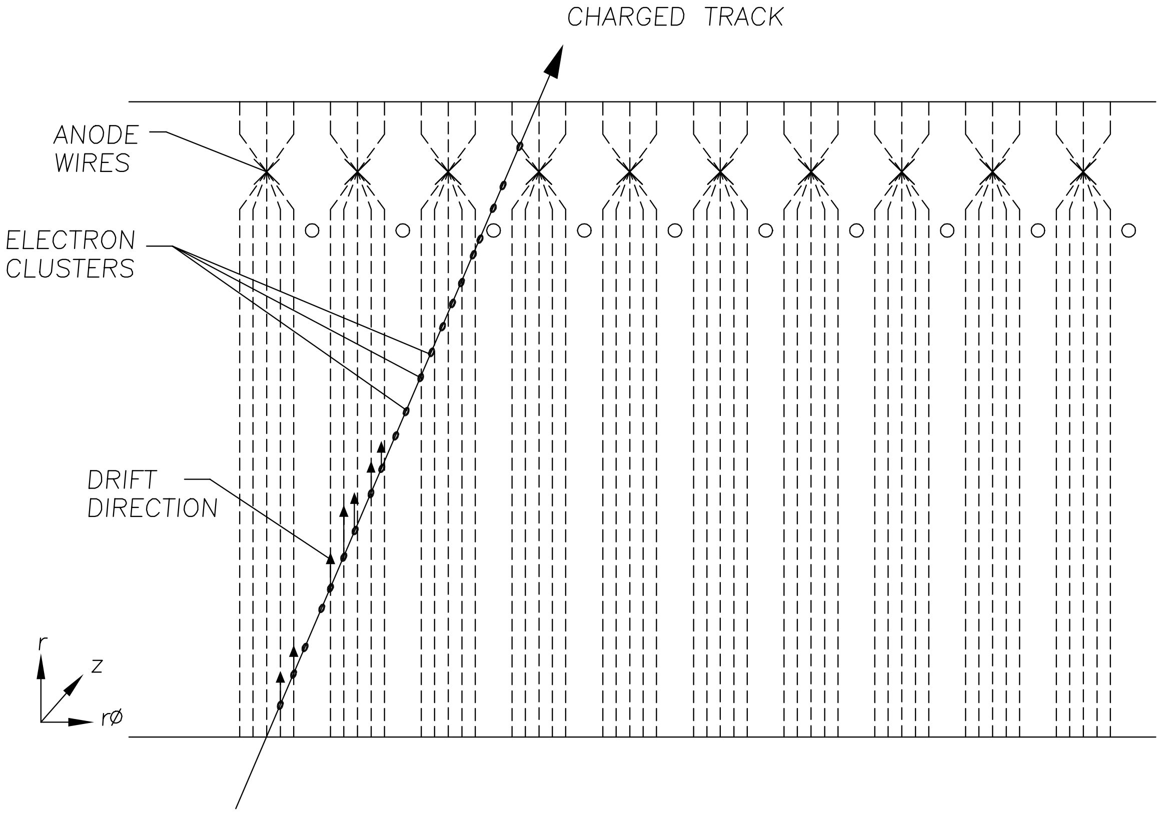

Figure 6.28: Diagram of TEC operation showing detector electric field lines and drift direction of electron clusters formed by ionizing particles.

and electrons at the BNL AGS. Data were taken in the summer of 1991 and 1992 to measure the track resolution of the prototype detector and the e/π separation over a momentum range of 700 MeV/c to 3.0 GeV/c. The detector used was a modified version of the NA-34 TRD instrumented with 6-bit FADC electronics. The prototype had an anode-cathode configuration similar to that of the PHENIX TEC design with the exception that the test detector only had a 1-cm drift space, whereas the PHENIX TEC will have a 3-cm drift space. The test results show a clear separation of the electron and pion distributions for the truncated mean distributions at 1 GeV/c and an e/π rejection of 0.01 for 90% electron efficiency (Fig. 6.29). The test results of e/π rejection verses momentum is shown in figure 6.30. Reconstructing charged tracks in the four plane prototype detector yielded a single point track resolution of 230 μm (Fig. 6.31).

The energy loss Monte Carlo calculates the dE/dx in the active gas volume of the TEC, and makes corrections for the expected detector and electronics responses, to predict the ability to measure energy loss signals. Energy loss through ionization in gases is well understood theoretically and has been checked and tested many times. To simulate the detector

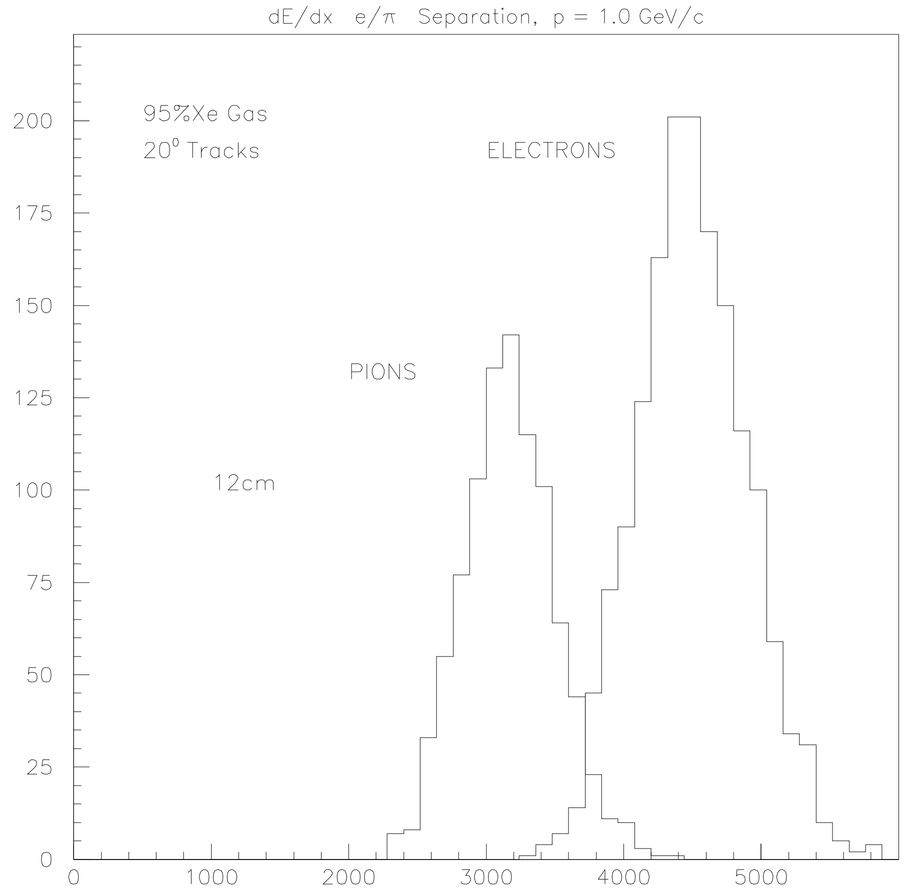

Figure 6.29: e/π separation at 1.0 GeV/c measured with the PHENIX TEC prototype.

response, the active gas space of each chamber was divided into 500 μm layers in the direction parallel to the anode plane. The ionization loss was modeled after the procedure in Asoskov et al. [8], which used formulas based on the oscillation strength function that can be calculated from experimental measurements of the cross sections for photoabsorption [1]. This formulation can be used to calculate the number of particle interactions with gas molecules, the energy transferred to the molecule in each interaction, and the point of interaction along the particle track. The Monte Carlo also includes the probabilities to deexcite gas molecules and to produce δ-electrons over a certain energy threshold.

Wherever the charged particle interacts, the Monte Carlo created an excited molecule and transferred kinetic energy to the ionized electron. The history of each δ-electron and photoelectron was followed. Its direction, interaction, Bragg behavior and multiple scattering were considered. The charged particle interaction was traced throughout the gas volume, and its energy deposits were then corrected for anode wire position, energy resolution, electronics

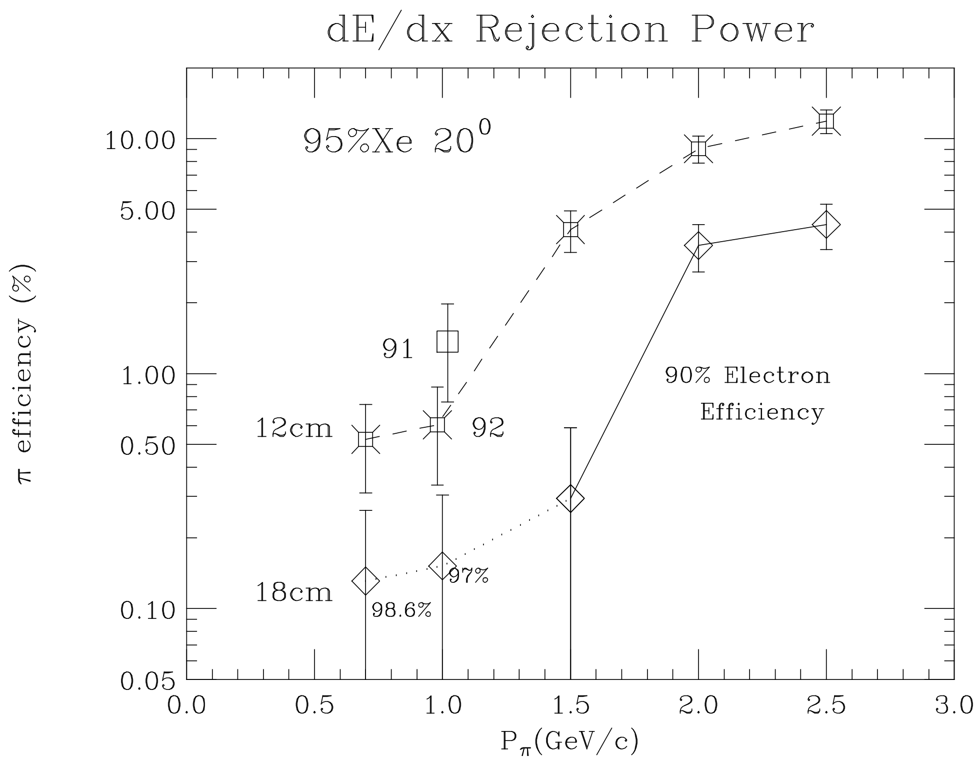

Figure 6.30: Pion rejection vs. momentum of TEC for 90% electron efficiency.

parameters to simulate detector response. The Monte Carlo predictions were then compared to test results from PHENIX prototype detectors.

The energy loss simulations predict an e/π separation of 5×10^{-3} at 600 MeV/c and 0.02 at 2.0 GeV/c for a four-plane PHENIX TEC (Fig. 6.32). The predictions of the simulation are in agreement with the test beam results using the prototype.

6.4.4 Cost

The cost of the TEC and its electronics is broken down by WBS item and is shown in Table 6.6.

6.4.5 Schedule

The proposed schedule for the TEC construction is shown in Fig. 6.33. It shows projected time required for design, prototyping, construction, and commissioning of both the chambers and of the electronics. As in the case for the other PHENIX tracking subsystems, the fabrication of the TEC for the first arm precedes the fabrication for the second arm.

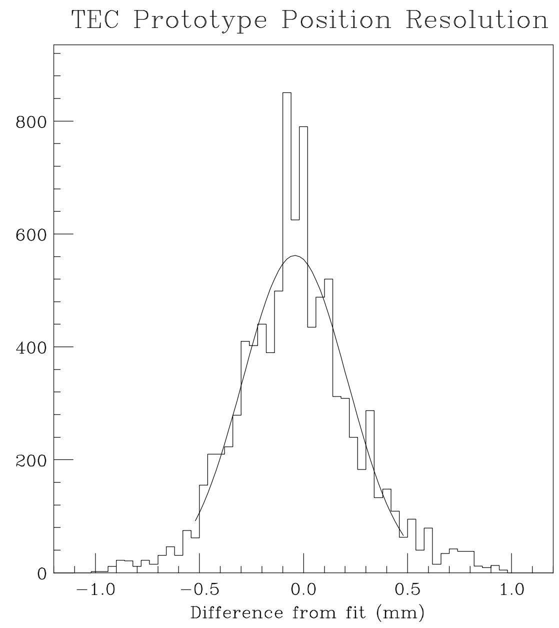

Figure 6.31: Single point, single track resolution of the PHENIX TEC prototype.

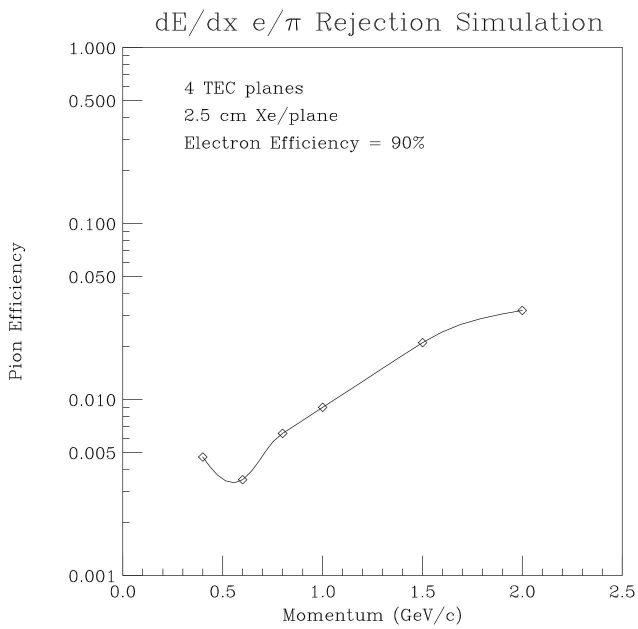

Figure 6.32: Simulation results of e/π rejection of PHENIX TEC.

Table 6.6: Cost Estimate for the PHENIX Time Expansion Chamber

		Amounts in FY93 k$					
W B S	Description	Total	M&S	EDIA	Labor	Cont%	Cont(k$)
5. 3. 3	**TEC System**	**2264**	**1720**	**144**	**448**	**20**	**453**
5. 3. 3	**Time Expansion Chambers**	**941**	**540**	**144**	**257**	**28**	**267**
5. 3. 3. 0	EDIA	144	0	144	0		36
5. 3. 3. 1	Prototyping	20	20	0	0		20
5. 3. 3. 2	Fabrication	693	520	0	173		194
5. 3. 3. 3	Testing	48	0	0	48		10
5. 3. 3. 4	Installation	36	0	0	36		7
5. 8. 1. 3. 3	**TEC Electronics**	**1323**	**1180**	**0**	**192**	**14**	**185**
5. 8. 1. 3. 3. 0	EDIA	0	0	0	0		
5. 8. 1. 3. 3. 1	Prototypes	120	20	0	100	58	70
5. 8. 1. 3. 3. 2	Fabrication	1179	1130	0	49	8	93
5. 8. 1. 3. 3. 3	Testing	24	0	0	24	50	12

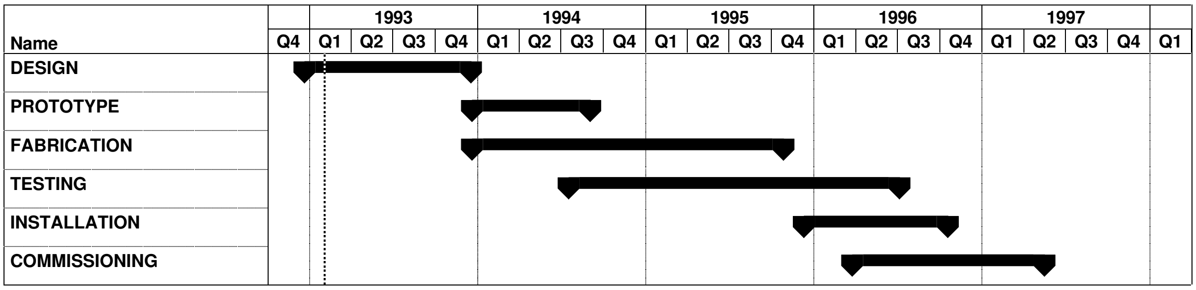

Figure 6.33: Overall schedule for the PHENIX time expansion chamber.

6.5 System Performance

6.5.1 Momentum and Mass Resolution

Calulations of the momentum and mass resolution of the PHENIX central tracking detector were performed. The detector components in the calculation are shown in Fig. 6.2. The transverse momentum resolution shown in Fig. 6.34 has $\Delta p_T/p_T$ plotted for electrons and kaons as function of their p_T. The p_T resolutions were calculated by using single tracks of known momenta, propagating them through the spectrometer, using GEANT to account for physical processes such as multiple scattering and energy loss. Hits were recorded at the intersections of the track and the detectors, and this information was used to reconstruct